UCRL-JRNL-208789

The Community Climate System Model: CCSM3

W. D. Collins, M. Blackmon, C. Bitz, G. Bonan, C. S. Bretherton, J. A. Carton, P. Chang, S. Doney, J. J. Hack, J. T. Kiehl, T. Henderson, W. G. Large, D. McKenna, B. D. Santer, R. D. Smith

December 29, 2004

Journal of Climate

The Community Climate System Model: CCSM3

William D. Collins[1]*, Maurice Blackmon[1], Cecilia Bitz[2], Gordon Bonan[1], Christopher S. Bretherton[2], James A. Carton[3], Ping Chang[4], Scott Doney[5], James J. Hack[1], Jeffrey T. Kiehl[1], Thomas Henderson[1], William G. Large[1], Daniel McKenna[1] Benjamin D. Santer[6], and Richard D. Smith[7]

[1] National Center for Atmospheric Research, Boulder, Colorado 80307
[2] University of Washington, Seattle Washington 98195
[3] University of Maryland, College Park, Maryland 20742
[4] Texas A&M University, College Station, Texas 77843
[5] Woods Hole Oceanographic Institution, Woods Hole, Massachusetts 02543
[6] Lawrence Livermore National Laboratory, Livermore, California 94551
[7] Los Alamos National Laboratory, Los Alamos, New Mexico 87545

December 3, 2004

Abstract

A new version of the Community Climate System Model (CCSM) has been developed and released to the climate community. CCSM3 is a coupled climate model with components representing the atmosphere, ocean, sea ice, and land surface connected by a flux coupler. CCSM3 is designed to produce realistic simulations over a wide range of spatial resolutions, enabling inexpensive simulations lasting several millenia or detailed studies of continental-scale climate change. This paper will show results from the configuration used for climate-change simulations with a T85 grid for atmosphere and land and a 1-degree grid for ocean and sea-ice. The new system incorporates several significant improvements in the scientific formulation. The enhancements in the model physics are designed to reduce or eliminate several systematic biases in the mean climate produced by previous editions of CCSM. These include new treatments of cloud processes, aerosol radiative forcing, land-atmosphere fluxes, ocean mixed-layer processes, and sea-ice dynamics. There are significant improvements in the sea-ice thickness, polar radiation budgets, equatorial sea-surface temperatures, ocean currents, cloud radiative effects, and ENSO teleconnections. CCSM3 can produce stable climate simulations of millenial duration without ad hoc adjustments to the fluxes exchanged among

*NCAR, P.O. Box 3000, Boulder, CO. 80307, email: wcollins@ucar.edu

the component models. Nonetheless, there are still systematic biases in the ocean-atmosphere fluxes in western coastal regions, the spectrum of ENSO variability, the spatial distribution of precipitation in the Pacific and Indian Oceans, and the continental precipitation and surface air temperatures. We conclude with the prospects for extending CCSM to a more comprehensive model of the Earth's climate system.

1. Introduction

The Community Climate System Model (CCSM) is a coupled model for simulating past, present, and future climates. In its present form, CCSM consists of four components for the atmosphere, ocean, cryosphere and land surface linked through a coupler that exchanges fluxes and state information among these components. It is developed and used by an international community of students and scientists from universities, national laboratories, and other institutions. Applications include studies of interannual and interdacadal variability, simulations of paleoclimate regimes, and projections of future anthropogenic climate change for international assessments. The most recent version, CCSM3, has been released to the climate community on 23 June, 2004. This paper describes some of the most important advances in model physics and dynamics, improvements in the simulated climate, and remaining scientific challenges for future development of CCSM.

CCSM3 is the third generation in an ongoing series of coupled models developed through international collaboration. The first generation, the Climate System Model version 1 (CSM-1), was released in 1996 (Boville and Gent 1998). This model was noteworthy since it did not require adjustments to the fluxes exchanged among the physical components in order to simulate stable, relatively drift-free climates. The second generation, the Community Climate System Model version 2 (CCSM2), was released in 2002 (Kiehl and Gent 2003). The climate simulated with CCSM2 exhibited several improvements over the climate generated from CSM1. The new model produced better simulations of extratropical sea surface temperatures, better tropical variability, and more realistic land surface temperatures. However, several important deficiencies prompted a new cycle of development that has resulted in CCSM3. The main model biases in CCSM2 include a double ITCZ and extended cold tongue; overestimation of winter land surface temperatures; underestimation of of tropical tropopause temperatures; erroneous cloud response to SST changes;errors in the east Pacific surface energy budget; and underestimation of tropical variability. As we will show, the new model has reduced or eliminated some of these biases.

This overview and the subsequent papers will focus on a configuration of CCSM with atmosphere and land models on Eulerian spatial grids T85 spectral truncation and ocean and sea-ice models with 1-degree lateral resolution at the equator (Appendix A), This configuration has been applied to simulations for international climate-change assessments. Lower-resolution versions of CCSM have been developed for applications including rapid scientific development, simulations of biogeochemical processes requiring multi-century simulations for equilibration, and studies of deep-time paleoclimate regimes. The sensitivity of the simulated climate to model resolution is discussed in Hack and Etcetera (2004), Yeager et al. (2004), Otto-Bliesner et al. (2004), and DeWeaver and Bitz (2004).

Basic features of the mean climate and its stability are discussed in this paper. Detailed analyses of the variability and transient behavior of the systems are presented in Deser et al. (2004), Alexander et al. (2004), Meehl et al. (2004), and Gent et al. (2004). Major improvements in the component models are outlined in section 2. Thorough descriptions of the enhancements in individual components are given elsewhere in this special issue (Collins et al. 2004b; Large et al. 2004, e.g.,). Improvements in the climate simulation and reductions in systematic errors relative to CCSM2 are discussed in section 3. The stability of the mean climate and analysis of secular trends in climate parameters are presented in section 4. Some of the most significant challenges for improving the simulations in future versions of CCSM are discussed in section 5. Plans for further development and extension to coupled chemistry-climate applications are presented in section 6.

2. Overview of CCSM3

The CCSM3.0 system includes new versions of all the component models. The model versions are CAM version 3.0 (Collins et al. 2004c,b), CLM version 3.0, CSIM version 5.0 (Briegleb et al. 2004), and POP version 1.4.3. New features in each of these components are described below.

a. *Design for multiple resolutions and atmospheric dynamics*

CCSM3 has been designed to produce simulations with reasonable fidelity over a wide range of resolutions and with a variety of atmospheric dynamical frameworks. This is accomplished by introducing dependence on resolution and dynamics in the time step and twelve other adjustable parameters in CAM3 (Collins et al. 2004c). With one exception, those parameters affect the physics governing clouds and precipitation in the atmosphere.

The standard version of CAM3 is based upon the Eulerian spectral dynamical core with triangular spectral truncation at 31, 42, and 85 wavenumbers. The zonal resolution at the equator ranges from 3.75° to 1.41°for the T31 and T85 configurations. It is also possible to integrate CCSM3 with a finite-volume dynamical core (Lin and Rood 1996, 1997) at 2 by 2.5-degree resolution, although at present this variant of CCSM3 is an experimental version requiring further refinement. The vertical dimension is treated using 26 levels with a hybrid coordinate. The land model is integrated on the same horizontal grid as the atmosphere, although each grid box is further divided into a hierarchy of land units, ground cover, and plant types. There are ten sub-surface soil layers in CLM3.

The ocean model uses a dipole grid with a horizontal resolution of 3° or 1°. The semi-analytic grids have the first pole located at the true South Pole and the second pole located over north America (Smith et al. 1995). The vertical dimension is treated using a height (z) coordinate with 25 levels extending to 4.75 in the 3-degree version and 40 levels extending to 5.37 km in the 1-degree version. The sea-ice model shares the same grid with the ocean model.

The three standard configurations CAM combine the T31 CAM/CLM with the 3° POP/CSIM, the T42 CAM/CLM with the 1° POP/CSIM, and the T85 CAM/CLM with the 1° POP/CSIM.

b. *Development the Atmosphere Component*

The new atmospheric model includes significant changes to the dynamics, cloud and precipitation processes, radiation processes, and treatments of aerosols. The finite volume dynamical core is now included as a standard option for integrating CAM (Boville et al. 2004). The tendency equations can be integrated with either process-split or time-split formulations of the numerical difference approximations (Williamson 2002). The physics of cloud and precipitation processes has been modified extensively (Boville and Etcetera 2004). The modifications include separate treatments of liquid and ice condensate; advection, detrainment, and sedimentation of cloud condensate; and separate treatments of frozen and liquid precipitation. The radiation has been updated with a generalized treatment of cloud geometrical overlap (Collins et al. 2001) and new treatment of longwave and shortwave interactions with water vapor (Collins et al. 2002a, 2004a). The prognostic sulfur cycle developed by Barth et al. (2000); Rasch et al. (2000) for predicting sulfate aerosols is now a standard option for the model. A prescribed distribution of sulfate, soil dust, carbonaceous species, and sea salt based upon a three-dimensional assimilation (Collins 2001; Rasch et al. 2001) is used to calculate the direct effects of tropospheric aerosols on the heating rates (Collins et al. 2002b). The corresponding effects of stratospheric volcanic aerosols are parameterized following (Ammann et al. 2003).

c. *Development of the Ocean Component*

The new ocean model includes modifications to the boundary layer physics and the numerical techniques for solving the barotropic continuity equations. The most significant modification is the inclusion of solar heating by chlorophyll based upon the parameterization by Ohlmann (2004). Transmissions vary spatially and are updated monthly. In contrast with the spatially uniform transmission factors used in CCSM2.0, subtropical oceans far from land are generally more transmissive while mid-latitude, coastal, and equatorial oceans are less transmissive. There are also minor modifications to the viscosities and diffusivities used in the K-profile parameterization (KPP) for vertical ocean mixing. In distinction with previous generations of CCSM, double diffusion associated with salt fingering is included by default in CCSM3.0. Air-sea exchanges of momentum, sensible heat, and latent heat are computed using the relative wind speed equal to the magnitude of the vector difference between the near-surface wind and the ocean surface currents. Finally the numerical algorithm for solving the barotropic equation has been replaced with a more efficient method to accelerate the computational performance of the ocean code.

d. *Development of the Land Component*

One of the primary objectives of the land developers has been to reduce the positive continental temperature biases during boreal winter. Modifications to the relationship between snow height and equivalent water depth, which have a significant impact on land-surface albedos (Oleson et al. 2003), have been considered but have not been adopted in CCSM3. The major change to the formulation of the biogeophysics increases the sensible and latent heat fluxes over vegetated surfaces. In previous versions of CCSM, the turbulent transfer coefficient between soil and the overlying canopy air was a constant for dense canopies. The new formulation makes this coefficient dependent on canopy density characterized by leaf and stem area indices (Oleson et al. 2004).. The transfer coefficient is used to obtain aerodynamic resistances for heat and moisture which are used to compute latent and sensible heat fluxes. Over large areas of Eurasia, these changes results in a reduction of the 2-meter air temperature by -1.5 to -2 K.

The new land model is based upon a nested subgrid hierarchy of scales representing land units, soil or snow columns, and plant functional types (PFTs) (Bonan et al. 2001; Oleson et al. 2004). CCSM3.0 includes the effects of competition for water among PFTs in its standard configuration.

e. *Development of the Sea-Ice Component*

The CSIM includes modifications to the formulation of ice dynamics, sea-ice albedos, and exchanges of salt between sea-ice and the surrounding ocean. The horizontal advection of sea ice is now treated with incremental remapping, a more accurate and efficient scheme than that used in previous versions(Libscomb and Hunke 2004). The momentum equation has been modified using scaling arguments to better simulate marginal ice under free drift (Connolley et al. 2004). The ice albedos have been empirically adjusted to yield better seasonal cycles of snow cover in the Arctic basin. The adjusted albedos are generally lower than the values adopted in CCSM2.0, although both sets of albedos are consistent with the ranges of observational estimates. The adjustments improve the rapid reduction in surface reflectivity during Arctic spring associated with snow melt. Exchange of sea salt with ocean water is included for ice melt, net congelation at ice base, net sublimation and condensation, and snow ice formation.

3. The mean coupled climate

There have been several significant improvements in the climate produced by CCSM3 relative to the climate simulated by CCSM2. These improvements are evident in a comparison of the control integrations of the two models for present-day conditions. In these comparisons, the mean climate produced by CCSM2 is represented by the average of years 900 to 1000 of its control simulation. This time period includes the interval that Kiehl and Gent (2003) used to describe the climate of CCSM2. For the CCSM2 control, the atmosphere and land are run at T42 resolution while the ocean and sea-ice are on a 1° grid. The mean climate produced by CCSM3 is represented by the average of years 400 to 500 from a control simulation using the model at its highest standard resolution (Appendix A). This time period is the same interval evaluated by Hurrell and Etcetera (2004). The comparison between the two integrations can change with time due to the secular trends in both runs (section 4 and Kiehl and Gent (2003)). However, the trends are sufficiently small that the major differences in, for example, sea-surface temperature are not appreciably affected.

a. *Energy balance at the surface and top of model*

The most significant change in radiation budget of CCSM3 is the disposition of solar radiation in the atmosphere. The atmosphere in CCSM3 absorbs 7.1 Wm^{-2} more shortwave radiation in clear-sky conditions and 7.9 Wm^{-2} more under all-sky conditions. The increased absorption is caused primarily the introduction of absorbing aerosol species (section b) and the updates to the extinction of near-infrared radiation by water vapor. The new aerosols increase the absorption by 2.8 Wm^{-2} for both clear-sky and all-sky conditions. The new treatment of near-infrared extinction by H_2O increases the clear and all-sky atmospheric atmospheric absorption by 4.0 and 3.1 Wm^{-2}, respectively. The enhanced absorption reduces the surface insolation by an equal amount. As a result, the net surface shortwave flux in CCSM3 is 9 Wm^{-2} smaller than that in CCSM2 (Figure 1). The new annual mean insolation of 160 Wm^{-2} is consistent with several empirical estimates (Kiehl and Trenberth 1997), although it is lower than the most recent ISCCP value of 166 Wm^{-2}(Zhang et al. 2004). Some of the largest discrepancies between model and ISCCP calculations occur in the tropics, where ISCCP overestimates the all-sky downwelling flux by 21 Wm^{-2} compared to surface radiometers.

Figure 1

The fidelity of the shortwave cloud forcing in CCSM3 to estimates from the Earth Radiation Budget Experiment (Harrison et al. 1990)[1] has improved, especially in the storm tracks. CCSM2 underestimated the magnitude of global annual-mean shortwave cloud forcing by 5.8 Wm^{-2}, while CCSM3 reproduces the ERBE estimates to within 0.1 Wm^{-2}. The largest zonal-mean differences occur in the storm tracks at 60N and 60S and in the tropical ITCZ between 10N and 10S. The increased forcing is in better agreement with the satellite data for the storm tracks and in slightly worse agreement for the tropics.

The all-sky and clear-sky surface longwave fluxes have decreased by 6.9 Wm^{-2} and 7.5 Wm^{-2}. The reductions in clear-sky flux in polar regions are related to the new longwave parameterization for water vapor (Collins et al. 2002a). These changes bring the model into much better agreement with in situ observations (Briegleb and Bromwich 1998).

b. *Sea surface temperature and salinity*

Several of the systematic errors in SSTs in CCSM2 have been reduced in CCSM3. Earlier versions of CCSM have consistently generated a region of equatorial water in the eastern Pacific which is colder than observed and extends too far west into the warm pool. The SSTs in this region have increased by between 1K and 2K in the central and western Pacific (Figure 2). A substantial fraction[2] of the SST increased is caused by the revisions to solar absorption by chlorophyll in the ocean mixed layer. The cold SST bias in the central equatorial Pacific exceeded 2K in CCSM2, and it is less than 1K in CCSM3. The equatorial SSTs in the warm pool are underestimated by between 0.2 to 0.5K. Figure 2

The CCSM2 also overestimates the SSTs by as much as 5K in narrow coastal regions just west of North and South America and southern Africa. This bias is not eliminated in CCSM3, but the SST errors have decreased by between 1K and 2K west of the American continents. The reductions in the biases result from better simulations of the observed insolation and surface stress, which leads to more coastal upwelling (section d).

The mean surface salinity errors in CCSM3 are -0.40 psu, a slight improvement over the corresponding error of -0.43 psu in CCSM2. One of the major areas of improvement is the equatorial surface salinity in the Pacific. In CCSM2, the western edge of the warm pool is two fresh by up to 2 psu [3], while the eastern edge too fresh by 0.5 to 1 psu. In CCSM3, the biases at both edges have been halved [4]. However, the equatorial Indian Ocean is too fresh by up to 2 psu, and the southern subtropical Pacific is too fresh by up to 1.5 psu. The precipitation in both of these regions relative to observations has increased from CCSM2 to CCSM3.

c. *Oceanic heat transport*

The meridional heat transport in CCSM3 is similar to the transports by mean flow in CCSM2. The maximum heat transport in the northern hemisphere is 2.2 PW [5], close to the 2 PW peak simulated by CCSM2 and comparable to recent observations (Kiehl and Gent 2003)(Figure 3). The maximum transport in the southern hemisphere is approximately 0.6 PW, somewhat lower than the 0.85 PW produced by CCSM2. In the southern hemisphere, the peak mean transport toward the equator is marginally weaker in CCSM3 than CCSM2. [6] Figure 3

d. *Oceanic circulations*

The representation of the equatorial Pacific undercurrent has improved in CCSM3. The realism of the simulated current can be evaluated against current measurements from the TOGA TAO buoy array (McPhaden et al. 1998). Previous versions of CCSM have tended to underestimate the strength of the counter-current. In CCSM3, the velocity at the core exceeds 100 cm/s, which is slightly larger than the velocities measured from the array (Figure 4)[7] The simulated counter-current is displaced downward by XX m[8], but otherwise its vertical and meridional extent are in good agreement with Figure 4

[1] line 211: The comparison is actually against Trenberth-modified ERBE – need reference

[2] line 228: How much of heating of equatorial Pacific is due to revision in chlorophyll heating?

[3] line 242: Estimate of CCSM2 surf. salinity bias at 120E

[4] line 243: What is the east-west gradient in salinity error in CCSM3?

[5] line 249: Verify maximum Eulerian mean NHT using years 400-499,

[6] line 254: Need figure for the section c from OS on ocean heat transport.

[7] line 261: Figure is for years 571-600: need to replace with average for years 400-500. Also, what is the longitude averaging range?

[8] line 262: What is the vertical displacement of the equa. Pac. c.c. relative to obs?

observations.

e. *Sea-ice thickness and concentration*

The fidelity of Arctic sea-ice thickness and distribution have improved in CCSM3 relative to earlier versions of the model. The annual mean ice thickness is between 2 and 2.5m over the central Arctic basin, with thicknesses exceeding 3m in the Beaufort Sea (Figure 5)[9]. The measured sea-ice thickness ranges between 2–3m, and CCSM2 produced ice with a mean thickness of 1.5m, The high resolution version of CCSM3 reproduces the observed gradient in sea-ice thickness across the Arctic basin from the east Siberian to Beaufort Seas (DeWeaver and Bitz 2004). The sea-ice concentration is not significantly different from the concentrations simulated by CCSM2. Like CCSM2, CCSM3 overestimates the concentrations in the Labrador Sea (Figure 5). Both the intermediate and high-resolution versions of CCSM3 produce excessive sea-ice in the Sea of Okhotsk, although the bias is less manifest at the higher resolution. The amplitudes of the seasonal cycle in northern hemisphere ice area simulated by the intermediate and high-resolution versions of CCSM3 are larger than observed. The simulated summertime area of approximately 5×10^6 km^2 is in good agreement with observations. However, in winter the modeled sea ice area of 1.5×10^7 km^2 exceeds the observed area of approximately 1.2×10^7 km^2 (Weatherly et al. 1998).

Figure 5

In the southern hemisphere, the sea-ice produced by CCSM3 is slightly more extensive than the ice area from CCSM2. Since CCSM2 produces a larger ice pack than observed, the bias in surface area in CCSM3 is slightly worse. At the end of the CCSM3 control integration, the surface area is approximately 1.3×10^7 km^2 while the observed annual-mean surface area is approximately 1.0×10^7 km^2. CCSM3 slightly overestimates the observed austral summertime minimum in sea-ice area of 2.1×10^6 km^2. In the austral winter, the modeled maximum sea ice area of up to 2.0×10^7 km^2 significantly exceeds the observed maximum of 1.5×10^7 km^2 (Weatherly et al. 1998). The spatial distribution of sea-ice thickness, however, is in better agreement with the recent observational estimates of Timmermann et al. (2004).

f. *Climate sensitivity*

Climate sensitivity is a measure of how a simulated climate changes in response to external forcing. In its traditional definition, climate sensitivity is the increase in global-average annual-mean surface temperature when the atmospheric concentration of carbon dioxide is doubled. Although climate sensitivity is not a useful metric for regional climate change, it has proven to be a very useful index for categorizing the response of multi-model ensembles to a given climate-change scenario (IPCC 2001).

The equilibrium sensitivity of CCSM3 in its high-resolution configuration is $2.7 \pm X$K for an increase from 355 to 710 ppmv (Kiehl et al. 2004). This represents an increase of 23% over the equilibrium sensitivity of 2.2K for for CCSM2 (Kiehl and Gent 2003). The two factors contributing to the increased sensitivity are the changes to the cloud processes in CAM (section b) and the resolution-dependent tuning of the cloud processes (section a). The climate sensitivity of CCSM3 increases with increasing res-

[9]line 268: Redo sea ice figures using years 400-500 rather than years 401-410.

olution of the atmosphere and land models. This variation is directed related to the variation in cloud radiative feedbacks with resolution (Kiehl and Gent 2003).

4. Stability and long-term behavior of coupled integration

CCSM3 has been designed to provide stable simulation relatively free of secular trends under fixed boundary conditions. The stability in the model system is a important design objective for two reasons. First, the absence of large trends is a necessary but not sufficient test of the conservation of energy, mass, and total water content of each of the components. Second, drift-free simulations are required for some of the more demanding applications of the model, including simulations of the carbon cycle that require millenia to attain equilibrium. The stability can be addressed by examining the energy budget and other properties of an integration for present-day conditions during years 100 to 600 (Appendix A).

In order for the climate system to be in equilibrium, the exchange of radiative energy across the top of the atmospheric model (TOM) must be as close to zero as possible. The exchange of radiant energy is the difference between the net shortwave radiation absorbed by the system and the net longwave radiation emitted by the system. For CCSM3, the annual-mean and RMS TOM energy balance is -0.21 ± 0.28 Wm^{-2}. Since the sign convention on the TOM balance is positive downward, on average the CCSM3 loses energy under present-day conditions. This loss rate is nearly identical to the loss rate of -0.2 Wm^{-2} for CCSM2 (Kiehl and Gent 2003). For comparison, the annual-mean net solar radiation absorbed at TOM under all-sky condition is 234.21 Wm^{-2}. The energy imbalance in the system is equivalent to 0.08% of the net solar input. The TOM all-sky and clear-sky fluxes are relatively stable, with trends between -0.01 and -0.03 Wm^{-2}/century.

Similarly, equilibrium of the climate system requires that the global-mean surface energy balance also be as close to zero as possible. The exchange of energy among the atmosphere and surface components is the difference between the net downward all-sky shortwave radiation, the net upward all-sky longwave radiation, the latent heat flux, and the sensible heat flux. For CCSM3, the annual-mean and RMS surface energy balance is -0.23 ± 0.21 Wm^{-2}. The net energy absorbed by the atmosphere is just the difference between the TOM and surface energy balances. For CCSM3, the mean and RMS energy absorbed by the atmosphere is 0.02 ± 0.13 Wm^{-2}. The atmospheric model includes a correction applied at each time step that sets the absorbed energy to zero. In the absence of that correction, the time-mean global-average energy absorbed is -0.27 Wm^{-2}. This residual absorption is due to numerical dissipation and to energy imbalances introduced by approximations related to water vapor and its phase transformations.

Since the simulated climate system is slowly losing energy, the global mean surface temperature should decrease slowly with time. After an initial 100-year period required to equilibrate the Arctic sea ice, the surface temperature decreases by -0.011K per century. Most of this trend is manifested in the southern hemisphere between 30S and

90S, which cools at a rate of -0.04K per century. The temperatures in the tropics between 30S and 30N and the northern hemisphere between 30N and 90N increase by less than 2×10^{-4}K per century.

The trend in the global volume-mean ocean temperature is -0.05K per century (Figure 6). As in CSM1 (Boville and Gent 1998)[10], the initial ocean adjustment to the energy imbalances at TOM occurs well below the mixed layer (Figure 7).

Figure 6

Figure 7

The decrease in the temperature of the southern hemisphere can be explained either by the expansion of the southern sea-ice or by the persistent cooling of the deep ocean water upwelling adjacent to Antarctica. The trends in sea-ice is in the northern and southern hemispheres are -0.02×10^6 and 0.18×10^6 km[]^2 per century, respectively. These changes correspond to changes in ice concentration (expressed in percent) of -0.002% and 0.015% per century. The temperature trend can be decomposed into a sum of terms associated with the trends in the areas and temperatures of the southern ocean, southern sea-ice, and ice over Antarctica. The decomposition shows that 83% of the southern-hemisphere trend is determined by the increase in sea-ice area and the -18.6K temperature differential between the sea-ice and surrounding ocean.

The trend in the global volume-mean salinity is -6.2×10^{-5} psu/century. Compared to the global mean salinity of 34.72 psu, the trend in salinity is equivalent to a relative change of -2×10^{-4}% per century. This reduction in salinity is caused by the adjustment of the soil moisture in the deepest layers of the land model during the first 300 years of integration (Kiehl and Gent 2003). Excess deep soil moisture is gradually released to the oceans by river runoff. These trends are smaller in magnitude, but opposite in sign, to the changes in salinity in CCSM2 (Kiehl and Gent 2003).

5. Challenges for further development

While many features of the climate are simulated with greater fidelity by CCSM3 than CCSM2, there are still significant biases that should be addressed in future generations of CCSM. These systematic errors can be illustrated by comparing the CCSM3 control integration against observations and meteorological analyses for the present-day climate. The time period from the control simulation spans the same interval (years 400–500) used in the comparisons against CCSM2 (section 3).

a. *Representation of major modes of variability*

Figure in preparation – more detailed text to follow.

The basic characteristics of the ENSO episodes simulated by CCSM2 and CCSM3 are quite similar. Two of the most important properties are the total variance and power spectrum of SST anomalies in the central Pacific. The results for the Nino 3.4 region (5S to 5N, 120W to 170W) are representative of other regions in the tropical Pacific. The total variance for the smoothed monthly anomalies in the Nino 3.4 temperature for CCSM2, CCSM3, and meteorological analysis (Kistler et al. 2001) are XXK, YYK, and ZZK, respectively[11]. These results show that the SST variability associated with

[10]line 350: Do we have evidence of the largest changes being below the mixed layer in CCSM2?

[11]line 384: What are the Nino 3.4 variances for CCSM2, CCSM3, and the NCEP analysis?

ENSO events is similar in CCSM2 and CCSM3. The power spectra of the monthly SST anomalies are shown in Figure 8. The CCSM3, like CCSM2, tends to produce ENSOs with a periodicity of approximately two years. The observed ENSOs have a relatively broad spectrum spanning three to five years. Despite the excessive frequency of ENSOs in the model, the maximum power in the modeled and observed spectra agree to within XX%[12].

Figure 8

b. *Double ITCZ in the Atlantic and Pacific*

Like previous generations of this model, CCSM3 produces a double ITCZ in the tropical Pacific. The southern Pacific convergence zone (SPCZ) in the observations extends southeast from the warm pool into the central southern Pacific (Figure 9). In CCSM3, the SPCZ is replaced by a southern branch of the ITCZ that is nearly zonal in orientation. The error is particularly evident during JJA¡ when the real SPCZ is much weaker and less extensive than the modeled convection south of the equator. The model overestimates the local precipitation rate in both branches of the ITCZ by up to 10 mm/day. The maximum precipitation in the northern half of the warm pool is too intense, and it is displaced westward by approximately 30 degrees relative to the observed maximum.

Figure 9

c. *Biases in continental precipitation and temperature*

Although the temperature errors in CCSM3 are smaller than those in CCSM2, there are are still large biases in the 2m air temperatures for sub-Arctic continental regions during boreal winter. The temperatures relative to observations (Willmott and Matsuura 1995; Willmott and Robeson 1995) during DJF are overestimated by as 10K in parts of Alaska and northern Eurasia. The mean overestimate for sub-Arctic continental regions north of 50N during DJF is $+3.9$K. The magnitude of the local errors are generally smaller than those in CCSM2 (Kiehl and Gent 2003), In addition, there are significant deficits in precipitation in the southeast United Sates, Amazonia, and southeast Asia throughout the annual cycle (Figure 9). These biases cause dynamic models of vegetation to produce unrealistic distribution of plant phenotypes in the affected regions (Levis and Bonan 2004). For fixed vegetation, models of the terrestrial carbon cycle are very sensitive to both temperature and precipitation. Higher temperatures cause water limitation because of the non-linear response of evaporation. This effect slows plant growth, leading to higher atmospheric concentrations of CO_2. Higher precipitation causes both heterotrophic respiration and gross primary production (GPP, the total amount of energy fixed by all photosynthetic organisms) to increase. It is difficult to predict the net effect on CO_2 concentration since both processes are highly variable and their effects on CO_2 have opposite sign. Therefore when there are biases in both temperature and precipitation, it may be difficult to predict the sign of the change in atmospheric CO_2. For these reasons, it will be important to reduce these biases in future versions of CCSM. The biases in annual-mean precipitation for three regions are listed in Table 1. The underestimation of rainfall ranges between 24% and 28% for these areas. In order to improve the fidelity of the dynamic vegetation and terrestrial carbon models, it will be necessary to reduce these errors in future versions of CCSM.

Table 1

[12] line 390: Fill in the precent diff. between the peak powers in spectra for CCSM3 and analysis.

Table 1: Model precipitation for continental regions

Region	Region Box	Precipitation (mm/day)	Error (mm/day)	% Error (percent)
SE United States	30N–40N, 80W–100W	2.4	-0.75	-24
Amazonia	10S–10N, 60W–80W	4.5	-1.7	-28
SE Asia	10N–30N, 80E–110E	3.1	-1.0	-24

One option to reduce the the positive temperature biases during boreal winter is to use a relationship between snow albedo and equivalent water depth which is more consistent with satellite observations (Oleson et al. 2003).

d. *SST biases and related atmospheric issues in western coastal regions*

CCSM3 produces sea-surface temperatures for the western coastal regions that are warmer than observed (Figure 2). Experiments with earlier versions of the coupled model suggest that the biases in SSTs are caused by underestimates of surface stress and overestimates of surface insolation (*W. Large and G. Danabasoglu, personal communication*). These experiments also show that the biases in these areas affect the SST and precipitation over large portions of the Atlantic and Pacific basins. The weaker surface stress results in weaker cooling of the ocean mixed layer by Ekman pumping, and the excess insolation results in solar heating through absorption of penetrative sunlight. These biases occur in the oceans adjacent to southern Africa and south America. The CCSM3 is compared in Table 2 against observations and analyses for these two western coastal regions averaged over the annual cycle. The comparison includes estimates of SST (Rayner et al. 2003), surface stress (Kistler et al. 2001), and all-sky and clear-sky insolation denoted by $S_{\downarrow}$ and $S_{\downarrow,c}$, respectively (Zhang et al. 2004). In the coastal region adjacent to South America, there CCSM3 overestimates the SST by 3K. While earlier generations of CCSM overestimated the surface insolation off South America by more than 50 Wm^{-2} in the annual mean, CCSM3 tends to slightly underestimate the surface shortwave flux. The much smaller error in insolation results from several modifications to the cloud parameterizations introduced in CCSM3 (Boville and Etcetera 2004) to address this issue. The observational comparison suggests that the weak surface stress in CCSM3 may still partially explain the 3K error in SST. It should be noted that the surface produced by CCSM3 is stronger than that in CCSM2 by up to 0.1 Nm^{2} partly because of the increased resolution in the atmosphere (Hack and Etcetera 2004). The factors leading to the SST biases are examined further in Large et al. (2004).

Table 2

e. *The semi-annual SST cycle in the eastern Pacific*

CCSM3 produces a fairly strong semi-annual cycle for SST in the eastern tropical Pacific that does occur in the real climate system (Figure 10). The region where this

Figure 10

Table 2: Properties of western coastal ocean regions

Region	Source	SST (K)	Stress Nm^{-2}	$S_{\downarrow}$ Wm^{-2}	$S_{\downarrow,c}$ Wm^{-2}
Africa	Obs.	23.3	0.065	216.7	296.7
(20S–5S,5W–5E)	CCSM3	25.6	0.065	223.5	292.2
S. America	Obs.	20.3	0.071	214.3	300.4
(20S–5S,65W–55W)	CCSM3	23.3	0.057	209.6	296.8

discrepancy is particularly evident lies between 5N to 5S and 110W to 90W. The observational climatology for the seasonal cycle in SST for this region is derived from the Hadley Centre's sea ice and sea surface temperature (SST) data set, HadISST (Rayner et al. 2003). The annual and regional mean temperature from CCSM3 is 25.5C, and this compares well with the HadISST estimate of 25.2C. However, the simulated and observed seasonal cycles in the regional mean SST are quite different. The annual cycle in SST produced by CCSM3 is 1.7C, or 43% of the observed cycle, and it is shifted in phase approximately 1.4 months later in the year. The semi-annual cycle in SST produced by CCSM3 is 1.6C, which is 220% of the semi-annual cycle in the HadISST data set. In the model, the phase of the semi-annual cycle is displaced by 5.3 months relative to the phase of the annual cycle. In summary, the magnitude of the annual cycle is roughly half that observed while the magnitude of the semi-annual cycle is roughly twice that observed. The causes for these systematic biases in the model physics have not been identified.

f. *Underestimation of downwelling shortwave radiation in polar regions*

In the Arctic, CCSM3 underestimates the downwelling all-sky shortwave radiation at the surface throughout the annual cycle. The insolation is underestimated relative to in situ observations from the Surface Heat Budget of the Arctic (SHEBA) experiment (Persson et al. 2002) and to estimates from the International Satellite Cloud Climatology Project (ISCCP) (Zhang et al. 2004). For this comparison, the ISCCP data for 1984 to 2000 has been averaged to produce a climatology. Between 70N to 90N, the annual-mean downwelling shortwave fluxes for all-sky conditions are 91 Wm^{-2} from ISCCP and 78 Wm^{-2} from CCSM3. The corresponding annual-mean clear-sky fluxes differ by only -3.9 Wm^{-2}, or -3%. The fluxes during the JJA season are 214 Wm^{-2} from ISCCP and 169 Wm^{-2} from CCSM3. The corresponding JJA-mean clear-sky fluxes differ by only 8.5 Wm^{-2}, or 2.7%. Since the clear-sky fluxes are in good agreement, the underestimate of surface insolation by CCSM3 is caused by an overestimate of the surface shortwave cloud radiative effect. Further analysis will be required to identify the sources of this error in the modeled cloud amount, cloud condensate path, and cloud microphysical properties.

6. Conclusions

A new version of the Community Climate System Model, CCSM3, has been developed and released to the climate community. The improvements in the functionality include the flexibility to simulate climate over a wide range of spatial resolutions with greater fidelity. This paper documents the high resolution version used for international assessments of climate change. The atmosphere and land share a grid for the Eulerian spectral atmospheric dynamics running at T85 truncation. The ocean and sea-ice share a 1-degree grid with a displaced pole in the northern hemisphere.

The atmosphere incorporates new treatments of cloud and ice-phase processes; new dynamical frameworks suitable for modeling atmospheric chemistry; improved parameterizations of the interactions among water vapor, solar radiation, and terrestrial thermal radiation; and a new treatment of the effects of aerosols on solar radiation. The land model include improvements in land-surface physics to reduce temperature biases and new capabilities to enable simulation of dynamic vegetation and the terrestrial carbon cycle. The ocean model has been enhanced with new infrastructure for studying vertical mixing, a more realistic treatment of solar heating by chlorophyll, and improvements to the representation of the ocean mixed layer. The sea ice model includes improved schemes for the horizontal advection of sea ice and for the exchange of salt with the surrounding ocean. The software has been designed so that CCSM3 is readily portable to a wide variety of computer architectures.

The climate produced by high-resolution CCSM3 shows several significant improvements over the climates produced by previous generations of the model. These include reduced sub-Arctic surface temperature biases during boreal winter, reduced tropical SST biases in the Pacific, and a better representation of the equatorial countercurrent in the Pacific. The new atmosphere features smaller global biases in all-sky surface insolation; improved simulation of cloud radiative effects in the storm tracks and during ENSO events; smaller biases in upper tropical tropospheric temperatures (Collins et al. 2004b); and a more realistic surface radiation budget under clear-sky conditions. The sea ice features a much more realistic simulation of the spatial distribution of ice concentration and of ice thickness. The climate is stable over 500 years subject to perpetual present-day boundary conditions.

There are still several aspects that should be improved in future versions of CCSM. These include the periodicity of ENSO and its projections onto sea-level pressure and precipitation; the double ITCZ in the Pacific, and the large precipitations biases in the western Indian Ocean. Other major modes of variability that are not well-simulated include the Madden-Julian oscillation. The errors in continental precipitation and temperatures need to be addressed to facilitate modeling of dynamic vegetation and the terrestrial carbon cycle. While the representation of the surface fluxes in coastal regions west of Africa and South America has improved, there are still significant biases in the coastal SSTs. Reduction in these biases will affect the simulation over large areas of the Pacific and Atlantic basins. Finally, there are still significant errors in the radiative energy budget of polar regions. These affect both the seasonal cycle and the climate feedbacks of sea ice.

Research is underway to diagnose these biases at the process level and to test improvements in physics and dynamics that would improve the simulation fidelity. At

Table 3: Control Integrations using CCSM3

Resolution	Present (years)	1%CO_2/yr (years)	2×CO_2 (years)	4×CO_2 (years)	1780 (years)	1870 (years)	20th C (years)
T85_gx1v3	b30.009 (661)	b30.026 (161)	b30.026a (152)	b30.036b (153)	– (0)	b30.020 (235)	b30.030 (8×130)
T42_gx1v3	b30.004 (1001)	b30.025 (214)	b30.025a (301)	b30.025b (301)	b30.100 (499)	b30.043 (302)	– (0)
T31_gx3v5	b30.031 (748)	b30.032 (171)	b30.032a (157)	b30.032b (160)	b30.105 (433)	b30.048 (154)	– (0)

the same time, the model is being extended to include a comprehensive treatment of terrestrial and oceanic biogeochemistry and ecosystem dynamics. Detailed representations of reactive chemistry, photochemistry, and aerosol microphysics have been added to the atmosphere. These developments are the initial steps toward building a more comprehensive model of the entire Earth system that can be applied to climates of the past, present, and future.

A. Control integrations of CCSM3

A comprehensive suite of control experiments have been performed with CCSM3. The output from these experiments has been made available to the climate community and may be used without restriction. Each of the configurations has been integrated using the three standard configurations of CCSM (section a. The experiments include simulations under constant present-day and preindustrial conditions corresponding to 1780 and 1870. In order to characterize the sensitivity of the model to increased atmospheric concentrations of CO_2, the model has been integrated with a 1% increase in CO_2 per year starting from initial conditions obtained from the present-day run. Two other simulations have been branched from the transient 1%CO_2/year simulation when the decadal-mean CO_2 concentration is equal to two times and four times its present-day value. The CO_2 concentration is held fixed in each of these runs to the values at the branch points from the transient simulation. For the purposes of these control experiments, the present-day global-mean annually-averaged mixing-ratio of CO_2 is equal to 355 ppmv, its value in 1990.

The control integrations are shown in Table 3. The table lists the types of experiments, the resolution used in each integration, the length of each experiment in years, and the series identifier for each simulation. For more details regarding the types of model output available and the methods for access to these data, please contact the CCSM3 data working group [13]. The control experiment discussed in this paper is b30.009. Table 3

[13] line 558: correct?

Acknowledgement The authors wish to acknowledge members of the CCSM Software Engineering Group and NCAR's Divisions for Climate and Global Dynamics, Atmospheric Chemistry, and Scientific Computing for their substantial contributions to the development of CCSM3.

The new model would not exist without the significant input from members of the CCSM working groups for software engineering and the component models for the atmosphere, land, ocean, and sea-ice too numerous to mention.

We would like to acknowledge the substantial contributions to the CCSM project from the National Science Foundation (NSF), Department of Energy (DOE), the National Oceanic and Atmospheric Administration, and the National Aeronautics and Space Administration.

This study is based on model integrations were performed by NCAR and CRIEPI with support and facilities provided by NSF, DOE, MEXT, and ESC/JAMSTEC.

References

Alexander, M. A., G. Branstator, A. Capotondi, C. Cassou, R. I. Cullather, Y.-O. Kwon, J. R. Norris, and I. Wainer, 2004: Extra-tropical coupled ocean-atmosphere variability. *J. Clim.*, *this issue*.

Ammann, C. M., G. A. Meehl, W. M. Washington, and C. S. Zender, 2003: A monthly and latitudinally varying volcanic forcing dataset in simulations of 20th century climate. *Geophys. Res. Lett.*, **30**, 1657, doi:10.1029/2003GL016875.

Barth, M. C., P. J. Rasch, J. T. Kiehl, C. M. Benkovitz, and S. E. Schwartz, 2000: Sulfur chemistry in the National Center for Atmospheric Research Community Climate Model: Description, evaluation, features and sensitivity to aqueous chemistry. *J. Geophys. Res.*, **105**, 1387–1415.

Bonan, G. B., S. Levis, L. Kergoat, and K. W. Oleson, 2001: Landscapes as patches of plant functional types: An integrating approach for climate and ecosystem models. *Glob. Biogeochem. Cycles*, **16**, 5.1–5.23.

Boville, B. A. and Etcetera, 2004: The impact of changing moist physical processes on the general circulation of CAM: Sensitivity studies. *J. Clim.*, *this issue*.

Boville, B. A. and P. R. Gent, 1998: The NCAR Climate System Model, Version One. *J. Clim.*, **11**, 1115–1130.

Boville, B. A., P. J. Rasch, and Etcetera, 2004: Effect of numerical formulation of FV atmospheric dynamics on the atmospheric general circulation. *J. Clim.*, *this issue*.

Briegleb, B. P., C. M. Bitz, E. C. Hunke, W. H. Lipscomb, M. M. Holland, J. L. Schramm, and R. E. Moritz, 2004: Scientific description of the sea ice component in the Community Climate System Model, Version Three. Technical Report NCAR/TN-463+STR, National Center for Atmospheric Research, Boulder, CO. 80307-3000, 78 pp.

Briegleb, B. P. and D. H. Bromwich, 1998: Polar radiation budgets of the NCAR CCM3. *J. Clim.*, **11**, 1246–1286.

Collins, W. D., 2001: Parameterization of generalized cloud overlap for radiative calculations in general circulation models. *J. Atmos. Sci.*, **58**, 3224–3242.

Collins, W. D., J. K. Hackney, and D. P. Edwards, 2002a: A new parameterization for infrared emission and absorption by water vapor in the National Center for Atmospheric Research Community Atmosphere Model. *J. Geophys. Res.*, **107**, 8028, doi:10.1029/2000JD000032.

Collins, W. D., J. M. Lee-Taylor, D. P. Edwards, and G. L. Francis, 2004a: Effects of increased near-infrared absorption by water vapor on the climate system. *J. Geophys. Res.*, in preparation.

Collins, W. D., P. J. Rasch, B. A. Boville, J. J. Hack, J. R. McCaa, D. L. Williamson, B. P. Briegleb, C. M. Bitz, S.-J. Lin, M. H. Zhang, and Y. Dai, 2004b: The formulation and atmospheric simulation of the Community Atmosphere Model: CAM3. *J. Clim.*, *this issue*.

Collins, W. D., P. J. Rasch, B. A. Boville, J. J. Hack, J. R. McCaa, D. L. Williamson, J. T. Kiehl, B. Briegleb, C. Bitz, S.-J. Lin, M. Zhang, and Y. Dai, 2004c: Description of the NCAR Community Atmosphere Model (CAM3). Technical Report NCAR/TN-464+STR, National Center for Atmospheric Research, Boulder, Colorado 80307-3000, 226 pp.

Collins, W. D., P. J. Rasch, B. E. Eaton, D. W. Fillmore, J. T. Kiehl, T. C. Beck, and C. S. Zender, 2002b: Simulation of aerosol distributions and radiative forcing for INDOEX: Regional climate impacts. *J. Geophys. Res.*, **107**, 4664, doi: 10.1029/2001JD001365.

Collins, W. D., P. J. Rasch, B. E. Eaton, B. Khattatov, J.-F. Lamarque, and C. S. Zender, 2001: Simulating aerosols using a chemical transport model with assimilation of satellite aerosol retrievals: Methodology for INDOEX. *J. Geophys. Res.*, **106**, 7313–7336.

Connolley, W. M., J. M. Gregory, E. C. Hunke, and A. J. McLaren, 2004: On the consistent scaling of terms in the sea ice dynamics equation. *J. Phys. Oceanogr.*, 1776–1780.

Deser, C., A. Capotondi, and R. Saravanan, 2004: ENSO and tropical Atlantic variability in CCSM3. *J. Clim.*, *this issue*.

DeWeaver, E. and C. M. Bitz, 2004: Atmospheric circulation and Arctic sea ice in CCSM3 at medium and high resolutions. *J. Clim.*, *this issue*.

Gent, P. R., F. Bryan, D. Tsumune, K. Lindsay, G. Danabasoglu, M. Hecht, and S. C. Doney, 2004: Thermocline and deep ocean ventilation during the 20th century in the CCSM3. *J. Clim.*, *this issue*.

Hack, J. J. and Etcetera, 2004: Impacts of horizontal resolution on ccsm3. *J. Clim.*, *this issue*.

Harrison, E. F., P. Minnis, B. R. Barkstrom, V. Ramanathan, R. D. Cess, and G. G. Gibson, 1990: Seasonal variation of cloud radiative forcing derived from the Earth Radiation Budget Experiment. *J. Geophys. Res.*, **95**, 18687–18703.

Hurrell, J. W. and Etcetera, 2004: Dynamic circulation and variability. *J. Clim.*, *this issue*.

IPCC, 2001: *Climate Change 2001 : The Scientific Basis*. Cambridge University Press, ed., J. T. Houghton, Y. Ding, D. J. Griggs, M. Noguer, P. J. van der Linden, and D. Xiaosu, 944 pp.

Kiehl, J. T., W. D. Collins, J. J. Hack, and C. Shields, 2004: The climate sensitivity of CCSM3. *J. Clim.*, *this issue*.

Kiehl, J. T. and P. R. Gent, 2003: The Community Climate System Model, Version Two. *J. Clim.*, **17**, 3666–3682.

Kiehl, J. T. and K. E. Trenberth, 1997: Earth's annual global mean energy budget. *Bull. Am. Meteorol. Soc.*, **78**, 197–208.

Kistler, R., E. Kalnay, W. Collins, S. Saha, G. White, J. Woollen, M. Chelliah, W. Ebisuzaki, M. Kanamitsu, V. Kousky, H. van den Dool, R. Jenne, and M. Fiorino, 2001: The NCEP-NCAR 50-year reanalysis: Monthly means CD-ROM and documentation. *Bull. Am. Meteorol. Soc.*, **82**, 247–267.

Large, W. G., G. Danabasoglu, and I. Wainer, 2004: Attribution and implications of upper ocean biases in CCSM3. *J. Clim.*, *this issue*.

Levis, S. and G. B. Bonan, 2004: Evaluation of CLM parameterizations and CAM-CLM climate using the CLM-DGVM as a diagnostic tool. *J. Clim.*, *this issue*.

Libscomb, W. H. and E. C. Hunke, 2004: Modeling sea-ice transport using incremental remapping. *Mon. Wea. Rev.*, **132**, 1341–1354.

Lin, S.-J. and R. B. Rood, 1996: Multidimensional flux-form semi-Lagrangian transport schemes. *Mon. Wea. Rev.*, **124**, 2046–70.

— 1997: An explicit flux-form semi-Lagrangian shallow-water model on the sphere. *Q. J. R. Meteorol. Soc.*, **123**, 2477–2498.

McPhaden, M. J., A. J. Busalacchi, R. Cheney, J. R. Donguy, K. S. Gage, D. Halpern, M. Ji, P. Julian, G. Meyers, G. T. Mitchum, P. P. Niiler, J. Picaut, R. W. Reynolds, N. Smith, and K. Takeuchi, 1998: The tropical ocean global atmosphere observing system: A decade of progress. *J. Geophys. Res.*, **103**, 14169–14240.

Meehl, G. A., J. M. Arblaster, D. M. Lawrence, E. K. Schneider, and A. Seth, 2004: Monsoon regimes in CCSM3. *J. Clim.*, *this issue*.

Ohlmann, J. C., 2004: Ocean radiant heating in climate models. *J. Clim.*, **16**, 1337–1351.

Oleson, K. W., G. B. Bonan, C. Schaaf, F. Gao, Y. Jin, and A. Strahler, 2003: Assessment of global climate model land surface albedo using MODIS data. *Geophys. Res. Lett.*, **20**, 1443, doi:10.1029/2002GL016749.

Oleson, K. W., Y. Dai, G. B. Bonan, M. Bosilovich, R. Dickinson, P. Dirmeyer, F. Hoffman, P. Houser, S. Levis, G.-Y. Niu, P. Thornton, M. Vertenstein, Z.-L. Yang, and X. Zeng, 2004: Technical description of the Community Land Model (CLM). Technical Report NCAR/TN-461+STR, National Center for Atmospheric Research, Boulder, CO. 80307-3000, 174 pp.

Otto-Bliesner, B. L., E. C. Brady, G. Clauzet, Z. Kothavala, S. Levis, and R. A. Tomas, 2004: Sensitivity of the climate system to glacial-interglacial forcing in CCSM3. *J. Clim.*, *this issue*.

Persson, P. O. G., C. W. Fairall, E. L. Andreas, P. S. Guest, and D. K. Perovich, 2002: Measurements near the Atmospheric Surface Flux Group tower at SHEBA: Near-surface conditions and surface energy budget. *J. Geophys. Res.*, **C107**, 8045, doi: 10.1029/2000JC000705.

Rasch, P. J., M. C. Barth, J. T. Kiehl, S. E. Schwartz, and C. M. Benkovitz, 2000: A description of the global sulfur cycle and its controlling processes in the National Center for Atmospheric Research Community Climate Model, Version 3. *J. Geophys. Res.*, **105**, 1367–1385.

Rasch, P. J., W. D. Collins, and B. E. Eaton, 2001: Understanding the Indian Ocean Experiment (INDOEX) aerosol distributions with an aerosol assimilation. *J. Geophys. Res.*, **106**, 7337–7356.

Rayner, N. A., D. E. Parker, E. B. Horton, C. K. Folland, L. V. Alexander, D. P. Powell, E. C. Kent, and A. Kaplan, 2003: Global analyses of sea surface temperature, sea ice, and night marine air temperature since the late nineteenth century. *J. Geophys. Res.*, **108**, 4407, doi:10.1029/2002JD002670.

Smith, R. D., S. Kortas, and B. Meltz, 1995: Curvilinear coordinates for global ocean models. Technical Report LA-UR-95-1146, Los Alamos National Laboratory.

Timmermann, R., A. Worby, H. Goosse, and T. Fichefet, 2004: Utilizing the aspect sea ice thickness data set to evaluate a global coupled sea ice-ocean model. *J. Geophys. Res.*, **C109**, C07017, doi:10.1029/2003JC002242.

Weatherly, J. W., B. P. Briegleb, and W. G. Large, 1998: Sea ice and polar climate in the NCAR CSM. *J. Clim.*, **11**, 1472–1486.

Williamson, D. L., 2002: Time-split versus process-split coupling of parameterizations and dynamical core. *Mon. Wea. Rev.*, **130**, 2024–2041.

Willmott, C. J. and K. Matsuura, 1995: Smart interpolation of annually averaged air-temperature in the United States. *J. Appl. Meteorol.*, **34**, 2577–2586.

Willmott, C. J. and S. M. Robeson, 1995: Climatologically aided interpolation (CAI) of terrestrial air-temperature. *International Journal Of Climatology*, **15**, 221–229.

Yeager, S. G., J. J. Hack, C. Shields, and W. G. Large, 2004: Low resolution CCSM3. *J. Clim.*, *this issue*.

Zhang, Y. C., W. B. Rossow, A. A. Lacis, V. Oinas, and M. I. Mishchenko, 2004: Calculation of radiative fluxes from the surface to top of atmosphere based on ISCCP and other global data sets: Refinements of the radiative transfer model and the input data. *J. Geophys. Res.*, **109**, D19105, doi:10.1029/2003JD004457.

This work was performed under the auspices of the U.S. Department of Energy by the University of California, Lawrence Livermore National Laboratory under Contract No. W-7405-Eng-48.

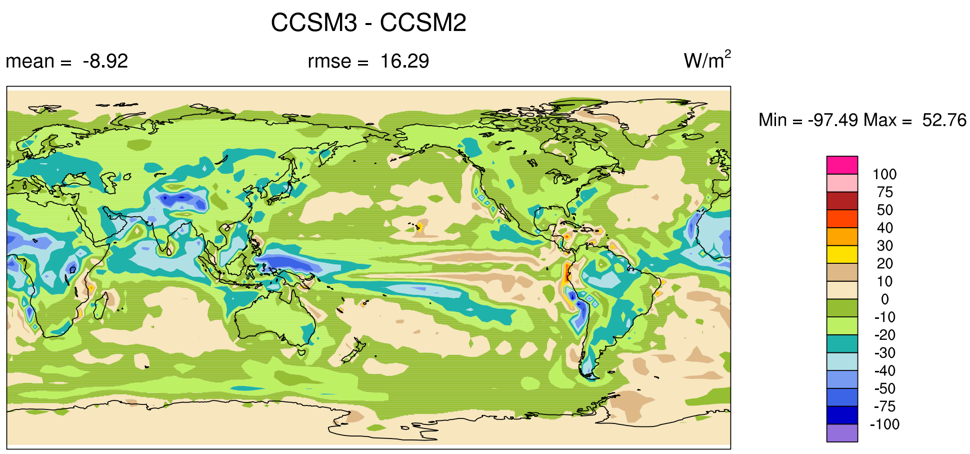

Figure 1: Difference in annual-mean net surface insolation between CCSM2 and CCSM3.

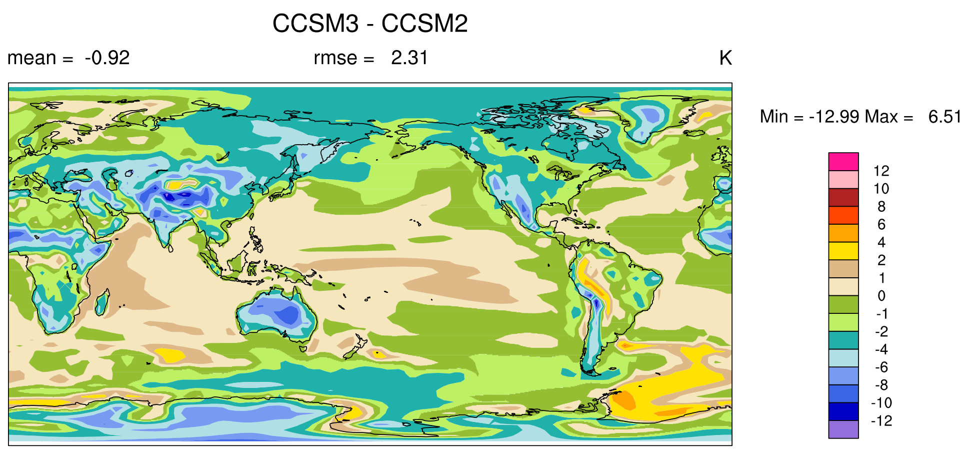

Figure 2: Difference in annual-mean surface temperature between CCSM2 and CCSM3.

Ocean Heat Transport Figure

Figure 3: Difference in annual-mean meridional ocean heat transport between CCSM2 and CCSM3.

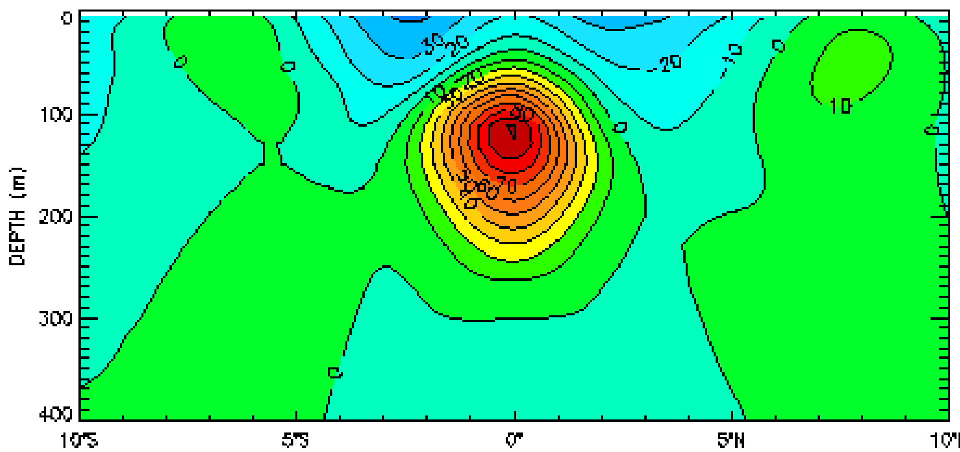

Figure 4: Difference in annual-mean zonal equatorial undercurrent (cm/s) in the Pacific.

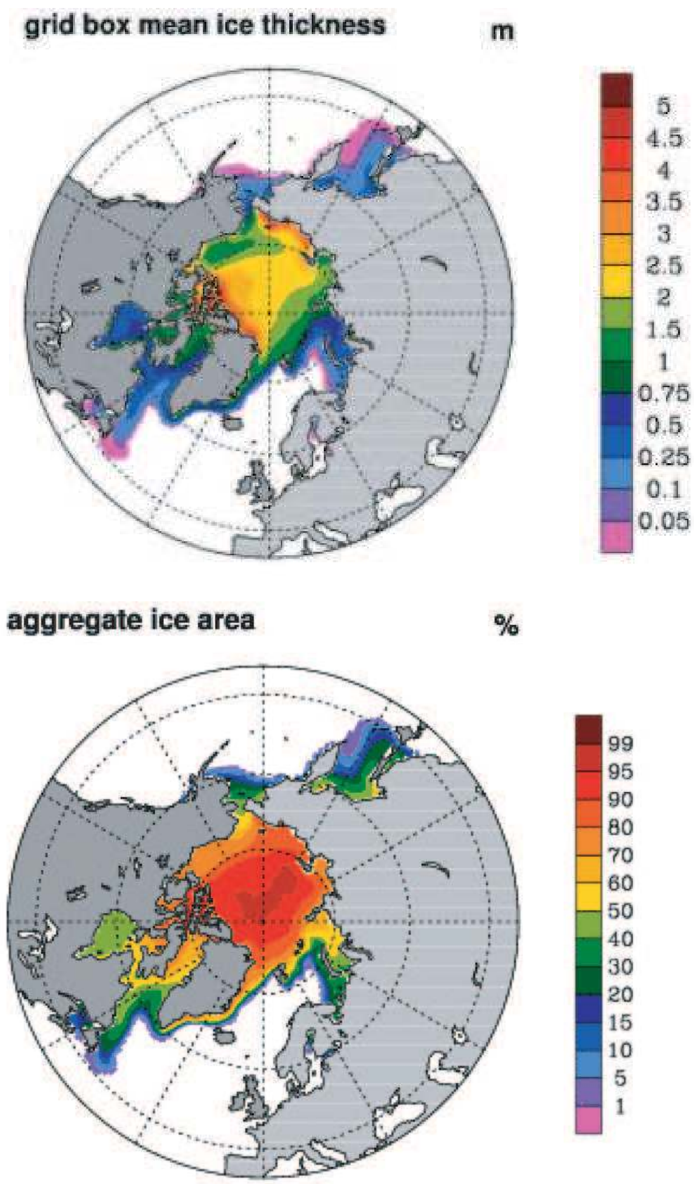

Figure 5: Annual-mean sea-ice thickness and concentration from CCSM3.

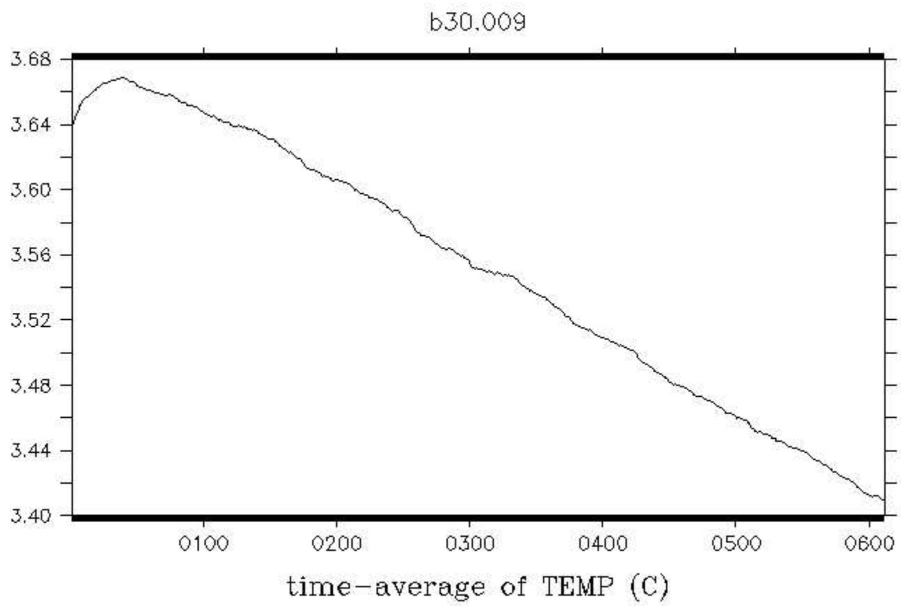

Figure 6: Annual-mean globally-averaged ocean potential temperature as a function of year of simulation.

Vertical X-section of Ocean Pot. Temp. vs Time

Figure 7: Global-mean ocean potentital temperature as a function of depth and year of simulation.

Power spectra of Nino 3.4 indices

Figure 8: Power spectra of the the Nino 3.4 indices for CCSM2, CCSM3, and the HadiSST(?) data set.

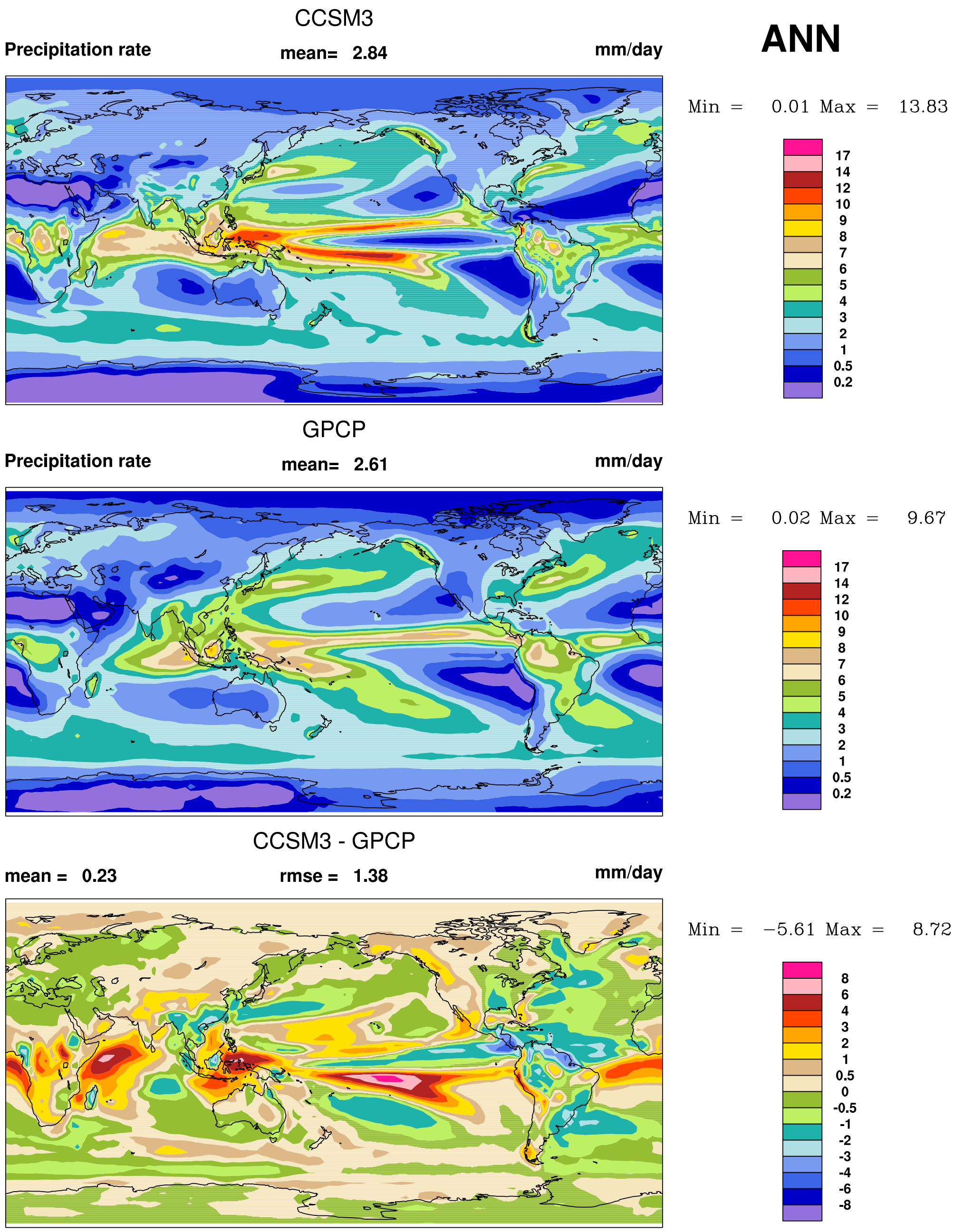

Figure 9: Annual-mean precipitation from CCSM3, the GPCP data set, and the difference between CCSM3 and GPCP.

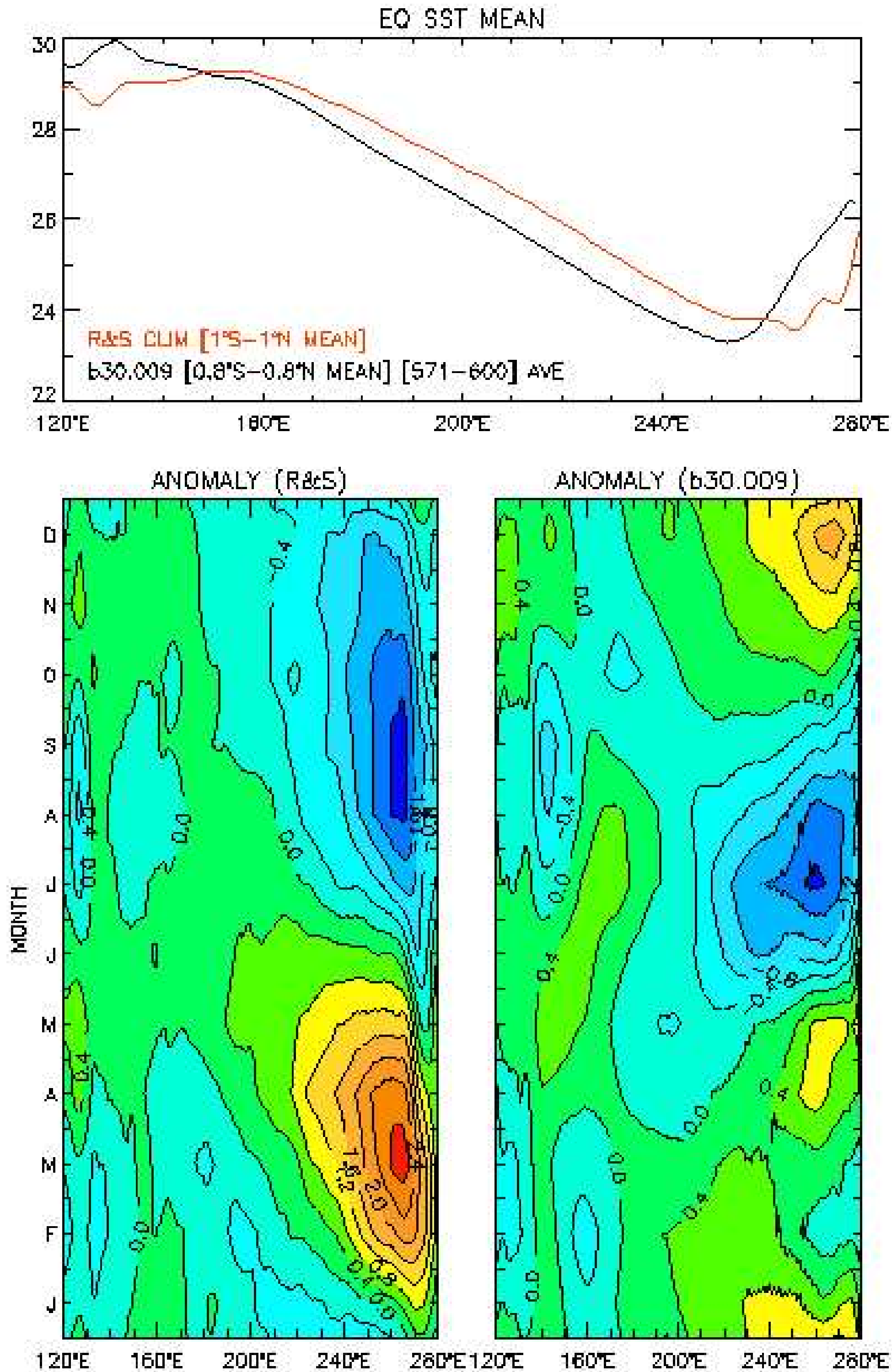

Figure 10: Seasonal cycle in surface temperature anomalies relative to the annual mean for 5S–5N and 120E–80W.